AFRL-RY-WP-TP-2012-0088

SEMICONDUTER OPTICAL AMPLIFIER AS A PHASE MODULATOR FOR COHERENT LASER RADAR (Preprint)

Jennifer Carns and Dr. Matthew Dierking

LADAR Technology Branch
Multispectral Sensing and Detection Division

Dr. Brad Duncan

University of Dayton

JANUARY 2012

AIR FORCE RESEARCH LABORATORY
SENSORS DIRECTORATE
WRIGHT-PATTERSON AIR FORCE BASE, OH 45433-7320
AIR FORCE MATERIEL COMMAND
UNITED STATES AIR FORCE

NOTICE AND SIGNATURE PAGE

*//Signature//

LAWRENCE J. BARNES
Project Manager
LADAR Technology Branch
Multispectral Sensing and Detection Division

//Signature//

BRIAN D. EWERT, Chief
LADAR Technology Branch
Multispectral Sensing and Detection Division

//Signature//

TRACY W. JOHNSTON, Chief
Multispectral Sensing and Detection Division
Sensors Directorate

REPORT DOCUMENTATION PAGE

Form Approved
OMB No. 0704-0188

1. REPORT DATE *(DD-MM-YY)*	2. REPORT TYPE	3. DATES COVERED *(From - To)*
January 2012	Journal Article Preprint	01 December 2009 – 01 December 2011

4. TITLE AND SUBTITLE

SEMICONDUTER OPTICAL AMPLIFIER AS A PHASE MODULATOR FOR COHERENT LASER RADAR (Preprint)

5a. CONTRACT NUMBER
IN-HOUSE

5b. GRANT NUMBER

5c. PROGRAM ELEMENT NUMBER
62204F

6. AUTHOR(S)

Jennifer Carns and Dr. Matthew Dierking (Multispectral Sensing and Detection Division, LADAR Technology Branch (AFRL/RYMM)
Dr. Brad Duncan (University of Dayton)

5d. PROJECT NUMBER
2003

5e. TASK NUMBER
11

5f. WORK UNIT NUMBER
2003112Y

7. PERFORMING ORGANIZATION NAME(S) AND ADDRESS(ES)

Multispectral Sensing and Detection Division
LADAR Technology Branch (AFRL/RYMM)
Air Force Research Laboratory, Sensors Directorate
Wright-Patterson Air Force Base, OH 45433-7320
Air Force Materiel Command, United States Air Force

University of Dayton
Electro-Optics Program
300 College Park
Dayton, OH, 45469-1620

8. PERFORMING ORGANIZATION REPORT NUMBER
AFRL-RY-WP-TP-2012-0088

9. SPONSORING/MONITORING AGENCY NAME(S) AND ADDRESS(ES)

Air Force Research Laboratory
Sensors Directorate
Wright-Patterson Air Force Base, OH 45433-7320
Air Force Materiel Command
United States Air Force

10. SPONSORING/MONITORING AGENCY ACRONYM(S)
AFRL/RYMM

11. SPONSORING/MONITORING AGENCY REPORT NUMBER(S)
AFRL-RY-WP-TP-2012-0088

12. DISTRIBUTION/AVAILABILITY STATEMENT
Approved for public release; distribution unlimited.

13. SUPPLEMENTARY NOTES
PAO Case Number: 88ABW 2012-1402, cleared 14 March 2012. This is a work of the U.S. Government and is not subject to copyright protection in the United States.

14. ABSTRACT

We investigate the use of a saturated semiconductor optical amplifier as a phase modulator for long range laser radar applications. The nature of the phase and amplitude modulation resulting from saturating in amplifier with a high peak power Gaussian pulse, and the impact this has on the ideal pulse response of a laser radar system is explored. We also present results of a proof-of-concept laboratory demonstration using phase modulated pulses to interrogate both a vibrating and a translating target.

15. SUBJECT TERMS

16. SECURITY CLASSIFICATION OF:			17. LIMITATION OF ABSTRACT:	18. NUMBER OF PAGES	19a. NAME OF RESPONSIBLE PERSON (Monitor)
a. REPORT	b. ABSTRACT	c. THIS PAGE			Lawrence Barnes
Unclassified	Unclassified	Unclassified	SAR	42	19b. TELEPHONE NUMBER *(Include Area Code)* N/A

Semiconductor Optical Amplifier as a Phase Modulator for Coherent Laser Radar

J. Carns[a,b], B. Duncan[b], and M. Dierking[a]

[a]Air Force Research Laboratory, 3109 Hobson Way, Bldg 622, WPAFB, OH 45433-7700

[b]Electro-Optics Program, University of Dayton, 300 College Park, Dayton, OH, 45469-1620

We investigate the use of a saturated semiconductor optical amplifier as a phase modulator for long range laser radar applications. The nature of the phase and amplitude modulation resulting from saturating an amplifier with a high peak power Gaussian pulse, and the impact this has on the ideal pulse response of a laser radar system is explored. We also present results of a proof of concept laboratory demonstration using phase modulated pulses to interrogate both a vibrating and a translating target.

I. Introduction

As synthetic aperture ladar systems yield resolutions higher than the diffraction limit, they offer a promising technology at ranges where traditional diffraction limited techniques are no longer effective. The first airborne SAL systems were demonstrated in a Defense Advanced Research Projects Agency/Air Force Research Laboratory program in 2006[1]. Pulses typically on the order of tens of microseconds in duration are transmitted, where the bandwidth necessary for the desired range resolution is obtained through linear frequency modulation (LFM) of the pulse. The goal of this work is to investigate a technique that will enable shorter pulse synthetic aperture ladar, as well as vibrometry.

Such a system would be less sensitive to target motion and ideally have a less complex system architecture by eliminating the hardware needed to implement LFM.

The technique we have investigated involves saturating a Semiconductor Optical Amplifier (SOA). This will not only amplify the transmitted pulse, but also induce a phase modulation. This phase modulation is typically regarded as undesirable, but by monitoring the transmitted pulse, the amplifier-induced phase modulation can be exploited as extra bandwidth to increase the range resolution of the transmitted pulse.

After presenting some background information and a summary of the signal model, the phase and amplitude characteristics of a SOA operated in the saturation regime will be explored in detail below. Results from a laboratory demonstration of SAL and vibrometry using transmitted pulses of this nature will then be presented, followed by our conclusions.

II. General System Description

The target area geometry is shown in Figure 1 (a). The target, located at point p, and the ladar are separated by a nominal range $R_{po} = \left(y_p^2 + z_p^2\right)^{1/2}$.

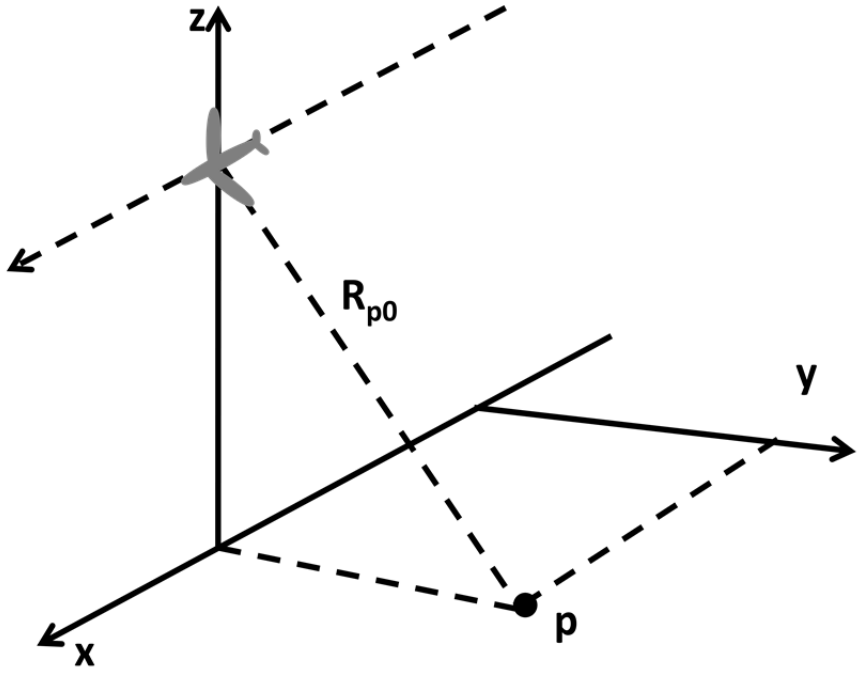

Figure 1. The target area geometry

The resolution in the range dimension is then determined by the bandwidth of the transmitted pulse, according to the relationship3

$$\Delta R = \frac{c}{2B}, \tag{1}$$

where c is the speed of light and B is the bandwidth of the transmitted pulse. In order to satisfy the Johnson criteria for tactical targets on the order of 2 m in size, a range resolution of ≤15 cm is desired[2]. To meet this requirement, a bandwidth of at least 1 GHz is necessary. This can be obtained through the transmission of a 1 ns FWHM transform limited pulse, or through the transmission of a longer pulse with sufficient phase modulation.

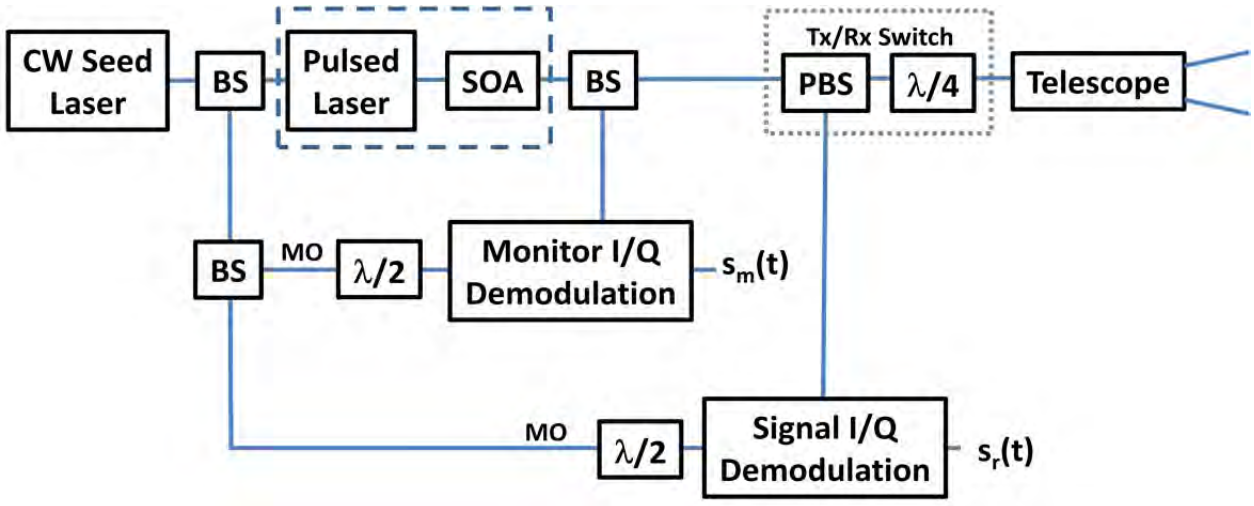

Figure 2. A potential architecture for the ladar system

For long range operation (tens of kilometers), a SOA can be used to increase the power of the transmitted pulse. One possible system architecture is depicted in Figure 1 (b), where a continuous wave laser serves as the master oscillator of the system and as a seed to the pulsed laser. A SOA is used to amplify the pulse, and a beamsplitter directs a portion of the signal to an I/Q demodulator, where it is decomposed into its in-phase (I) and quadrature (Q) components. The pulse then propagates through the transmit/receive switch to the target area. The return pulse, after passing through the transmit/receive switch, is directed to an I/Q demodulator. The return pulse and the stored monitor pulse can then be compared to yield information about the target.

If the SOA is operating in a saturated regime (that is, if the energy of the incoming pulse exceeds the saturation energy of the SOA) the pulse will experience modulation in both phase and amplitude. By monitoring the transmitted pulse, the phase modulation can be exploited as additional bandwidth to further improve the range resolution of the system. While the characteristics of the phase and amplitude modulation will be discussed in Sections V through VIII, the signal model and assumed processing techniques will be briefly summarized in the following two sections.

III. Range, Vibration , and SAL Processing

The transmitted optical signal can be expressed in complex exponential form as

$$\begin{aligned}\vec{s}_t(t) &= u_t(t)\exp\big(j\omega_c t + j\theta(t)\big)\left[\frac{1}{\sqrt{2}}\hat{x} + \frac{1}{\sqrt{2}}\exp\left(j\frac{\pi}{2}\right)\hat{y}\right] \\ &= s_b(t)\exp(j\omega_c t)\left[\frac{1}{\sqrt{2}}\hat{x} + \frac{1}{\sqrt{2}}\exp\left(j\frac{\pi}{2}\right)\hat{y}\right],\end{aligned} \tag{2}$$

where $u_t(t)$ is the envelope of the signal, ω_c is the carrier frequency, $\theta(t)$ represents any phase modulation of the transmitted pulse, $s_b(t)$ represents the baseband version of the transmitted signal, and where the signal has right-hand circular polarization due to the quarter waveplate in the transmit/receive switch. Upon interaction with a target, the polarization of the return signal becomes left-hand circular due to the change in direction of propagation, and the received signal is delayed by the roundtrip time $t_{rt} = 2R_p/c$. After passing through the quarter waveplate, the signal polarization becomes linear and the signal can be expressed as

$$\vec{s}_r(t) = u_t(t - t_{rt})\exp[j\omega_c(t - t_{rt}) + j\theta(t - t_{rt})] = s_b(t - t_{rt})\exp[j\omega_c(t - t_{rt})]\hat{x}. \tag{3}$$

For simplicity, it is assumed that the target has no affect on the envelope of the signal.

If the ladar and target have any vibrational or relative translational motion, the range to a target located at position (x_p, y_p, z_p), can be expressed as

$$R_p(t) = \sqrt{\big(v_t t - x_p\big)^2 + y_p^2 + z_p^2} + a_v \sin(\omega_v t) = R_{p0}\sqrt{1 + \frac{\big(v_t t - x_p\big)^2}{R_{p0}^2}} + a_v \sin(\omega_v t), \tag{4}$$

where we assume v_t is the relative translational velocity, a_v is the maximum vibrational displacement of the target toward the ladar system, ω_v is the frequency of the assumed sinusoidal vibration, and where translation has been limited to the x dimension of Figure 1. Assuming R_p is large with respect to all

other terms, the series expansion $(1+x)^n \cong 1+nx$, for x<<1 can be used on the first term of Equation (4) to yield

$$R_p(t) = R_{p0} + \frac{v_t^2 t^2}{2R_{p0}} - v_t t \frac{x_p}{R_{p0}} + \frac{x_p^2}{2R_{p0}} + a_v \sin(\omega_v t). \tag{5}$$

Noting that $t_{rt} = 2R_p/c$, inserting Equation (5) into Equation (3) yields

$$s_r(t) = s_b(t - t_{rt}) \exp(j\omega_c t)\exp(-j\phi_v)\exp(-j\phi_t)\hat{x}, \tag{6}$$

where

$$\phi_{\mathrm{v}} = \frac{4\pi}{\lambda} a_v \sin(\omega_v t) \tag{7}$$

is the phase accumulation associated with vibration and

$$\phi_{\mathrm{t}} = \frac{4\pi}{\lambda}\left(R_{p0} + \frac{v_t^2 t^2}{2R_{p0}} - v_t t \frac{x_p}{R_{p0}} + \frac{x_p^2}{2R_{p0}}\right) \tag{8}$$

is the phase accumulation associated with translational motion. The polarizing beamsplitter directs the received signal to the signal I/Q demodulator. The I/Q demodulator combines the signal and MO, and decomposes them into the in-phase and quadrature components $s_{Ir}(t)$ and $s_{Qr}(t)$, respectively. Assuming homodyne detection (i.e., the MO and the received signal are at the same carrier frequency) the composite received electrical signal is expressed as

$$s_r(t) = s_{Ir}(t) + j s_{Qr}(t) = u_{MO} s_b(t - t_{rt})\exp(-j\phi_v)\exp(-j\phi_t), \tag{9}$$

where u_{MO} is the amplitude of the CW MO. Here we have assumed $u_{MO} \gg u_t(t - t_{rt})$, and that AC coupling is used to filter out any DC terms. The monitor signal is also combined with the MO in the monitor I/Q demodulator, yielding the expression

$$s_m(t) = u_{MO} s_b(t). \tag{10}$$

Assuming conventional matched filtering techniques are used to detect the received pulse, the output of the matched filter for a single pulse is[3]

$$s_M(t) = \int_{-\infty}^{\infty} s_r(\tau) s_m^*(\tau - t) d\tau = \Im^{-1}\{S_r(\omega) S_m^*(\omega)\}, \tag{11}$$

where $s_r(t)$ is the received signal, the matched filter $s_m^*(-t)$ is the time reversed conjugate of the monitor signal, $S_r(\omega)$ and $S_m(\omega)$ are the Fourier transforms of the received and monitor signals, respectively, and $\Im^{-1}$ denotes the inverse Fourier transform operation. Since the transmitted pulse is monitored, an exact copy of each transmitted pulse is used to form the matched filter for the corresponding received pulse. In this case the filter is perfectly matched to the received signal and the output of the matched filter for a point target is referred to as the Ideal Point-Target Response, or IPR. The IPR is often characterized in terms of its Peak-to-Sidelobe Level Ratio (PSLR) and its Integrated Sidelobe Level Ratio (ISLR). The PSLR is the ratio of the peak power of the main lobe of the IPR to the peak power of the largest sidelobe of the IPR, while the ISLR is the ratio of the energy contained in the main lobe of the IPR to the energy contained in the sidelobes.

As will be discussed in Section IX, three laboratory demonstrations will be carried out. A stationary source will be used to interrogate a stationary target, a stationary vibrating target, and a translating target with no vibration.

If the ladar and target have no relative translational or vibrational motion, range processing can be carried out by substituting Equations (9) and (10) into Equation (11) such that

$$s_M(t) = u_{MO}^2 \exp\left(-j\frac{4\pi}{\lambda} R_{p0}\right) \mathcal{R}_{s_b}(t - t_{rt}) \tag{12}$$

where we have assumed the target is located at position $x_p = 0$. Note that the matched filter output contains a shifted version of the autocorrelation of the baseband transmitted signal, or

$$\mathcal{R}_{s_b}(t - t_{rt}) = \int_{-\infty}^{\infty} s_b(\tau - t_{rt}) s_b^*(t - \tau) d\tau. \tag{13}$$

The shape and width of the autocorrelation depends on the envelope and phase modulation of the transmitted signal. The degree to which the returns from two targets can be resolved in range depends on the range resolution of the system.

A vibrating target introduces an additional phase factor that can be exploited to yield further information about the nature of the target. For a vibrating target located at range R_p and cross-range location of $x_p = 0$, with no translational motion (i.e., $v_t = 0$), Equations (9) and (10) can be substituted into Equation (11), yielding

$$s_M(t) = \exp\left(-j\frac{4\pi}{\lambda}R_{p0}\right)\int_{-\infty}^{\infty} u_{MO}^2 s_b(\tau - t_{rt})\, s_b^*(\tau - t)\exp\left(-j\frac{4\pi}{\lambda}a_v \sin\big(\omega_v(\tau)\big)\right)d\tau. \quad (14)$$

Assuming the Doppler shift due to the vibration is approximately constant over the pulse duration such that $\phi_v(t) \approx \phi_v$, Equation (14) can be simplified to yield

$$s_M(t) = u_{MO}^2 \exp(-j\phi_v)\exp\left(-j\frac{4\pi}{\lambda}R_p\right)\mathcal{R}_{s_b}(t - t_{rt}), \quad (15)$$

Once again, the matched filter output contains a delayed version of the autocorrelation of the baseband signal. Furthermore, the phase of the matched filter output has a sinusoidal variation with a frequency equal to the vibrational frequency of the target. By interrogating the target with multiple pulses, the vibrational frequency of the target can be determined from the frequency at which the phase history varies, i.e. by taking a Fourier transform of the phase history. In this manner, the range to target as well as the vibrational frequency of the target can be determined.

Next, for a ladar that is translating with respect to a stationary target with no vibration (i.e., $\omega_v = 0$), the received signal from Equation (9) is expressed as

$$s_r(t,u) = u_t(t - t_{rt})u_{MO}\exp\big(j\theta(\tau - t_{rt})\big)\exp\left(-j\frac{4\pi}{\lambda}\left(R_{p0} + \frac{u^2}{2R_{p0}} - u\frac{x_p}{R_{p0}} + \frac{x_p^2}{2R_{p0}}\right)\right), \quad (16)$$

where $u = v_t t$. Since each pulse is transmitted from a different location, Equation (16) is really a function of the two coupled variables t and u, hence the notation $s_r(t,u)$. The fast-time variable t measures the range to target, and the slow time variable $u = vt$ yields information about the position of the target in the cross-range dimension (x), also known as the along-track dimension. Note that the phase associated with translation has an approximate quadratic variation in u.

SAL processing is generally carried out using a two-dimensional matched filter that is computed for an object in the center of the region of interest[3]. Here, the matched filter can be constructed using the stored transmitted pulses from the monitor, where the round-trip travel time and subsequent phase variation are calculated for a target located at position (x_0,y_0,z_0) in the center of the target area. The matched filter is then carried out as

$$s_M(t,u) = \Im^{-1}\{S_r(\omega,k_u)S^*_{t,0}(\omega,k_u)\}, \tag{17}$$

where $S_r(\omega,k_u)$ and $S^*_{t,0}(\omega,k_u)$ are the spatio-temporal Fourier transforms of the received signal and the matched filter, respectively. The output of the matched filter for a point target yields an IPR that is two dimensional, with the fast-time IPR yielding the location of the target in range, and the slow-time IPR yielding the location of the target in cross-range. Note that this analysis has assumed a single target located at position (x_p,y_p,z_p), but the theory can be extended to multiple targets by noting that the received signal in Equation (9) is actually a summation of the returns from each target in the region of interest.

The following sections will explore the behavior of a SOA when operated in the saturation regime, and the nature of the resulting phase modulation, which was identified as $\theta(t)$ in Equation (2). The matched filter processing techniques summarized in this section will then be used to obtain the fast-time IPR of the phase modulated transmitted pulse, and the effect on the range resolution of the system will be analyzed.

V. Operation of the Saturated Semiconductor Optical Amplifier

As a pulse travels through a semiconductor optical amplifier, it experiences gain due to the presence of an injection current which allows for the radiant recombination of electron-hole pairs and thus the stimulated emission of photons identical in amplitude and phase to the incident photons. If the incident power is large enough, the pulse saturates the amplifier, depleting the carriers. As the carrier density changes, the index of refraction experienced by the pulse also changes, which affects the shape of the pulse as well as its phase. These power and phase characteristics, derived in reference [4], are outlined in Equations (18) through (20), below.

It was shown that the power, $P_{out}(t)$, and phase, $\phi_{out}(t)$, of a pulse after propagating through a SOA can be expressed as

$$P_{out}(t) = P_{in}(t)\exp[h(t)] \tag{18}$$

and

$$\phi_{out}(t) = \phi_{in}(t) - \frac{1}{2}\alpha h(t), \tag{19}$$

where $P_{in}(t)$ is the input power, $\phi_{in}(t)$ is the input phase, α is the chirp parameter, and $h(t)$ is the integrated gain at each point along the pulse governed by the relationship

$$\frac{dh(t)}{dt} = \frac{g_0 L - h(t)}{\tau_c} - \frac{P_{in}(t)}{E_{sat}}\left[\exp\big(h(t)\big) - 1\right], \tag{20}$$

where g_0 is the small signal gain, L is the length of the active region, τ_c is the carrier lifetime, and E_{sat} is the saturation energy of the amplifier. The chirp parameter of Equation (19) is a dimensionless value that describes the magnitude of the phase change induced by the amplifier. It generally has a value

between 4 and 12, and it must be measured for each device [5]. Assuming the input pulse is Gaussian, the input power is expressed as

$$P_{in}(t) = \frac{E_{in}}{\tau_0\sqrt{\pi}} \exp\left(\frac{-t^2}{\tau_0^2}\right), \tag{21}$$

where τ_0 = 1.665· τ_p, and τ_p is the FWHM of the Gaussian input pulse. Equation (20) then becomes

$$\frac{dh(t)}{dt} = \frac{g_0 L - h(t)}{\tau_c} - \frac{E_{in}}{E_{sat}\tau_0\sqrt{\pi}} \exp\left(\frac{-t^2}{\tau_0^2}\right)\left[\exp\big(h(t)\big) - 1\right]. \tag{22}$$

For results presented in later sections, this equation, which must be solved numerically, was solved using the ode23t ordinary differential equation function in Matlab.

If the energy of the input pulse is high enough, the leading edge of the pulse depletes the carriers as the pulse travels through the SOA, thus saturating the gain, while the trailing edge of the pulse experiences a recovery in gain as the carriers repopulate the active region of the SOA. The time it takes for the carriers to repopulate is determined by the SOA's carrier lifetime, or gain recovery time. The carrier lifetime is generally on the order of a nanosecond[4]. As is evident in Equations (20) and (22), the key parameters that determine the phase and magnitude of the transmitted pulse are the SOA's carrier lifetime (τ_c), unsaturated gain (G_0), and chirp parameter (α), as well as the ratio of the input pulse energy to the saturation energy of the SOA (E_{in}/E_{sat}) and the input pulse duration (τ_p). Section VI will investigate the impact of the carrier lifetime and input pulse energy for a Gaussian pulse, and Section VII will address the impact of the unsaturated gain and the chirp parameter.

VI. Effects of the Carrier Lifetime and Input Energy

To explore the effects of the carrier lifetime, we assume a 1 ns FWHM Gaussian input pulse, a chirp parameter of α=6, an unsaturated gain of $G_0 = g_0 L = 30$ dB, and E_{in}/E_{sat} = 0.1. Equation (22) is

numerically solved in Matlab for a given value of the carrier lifetime, and the result, $h(t)$, is substituted into Equation (18) to yield the output pulse power. The results for carrier lifetimes of 0.1 ns and 2.0 ns are shown in Figure 2 (a). Each pulse is normalized to compare the pulse shapes against one another, and the dotted line represents the normalized 1 ns FWHM Gaussian input pulse as calculated by Equation (21). As can be seen, the carrier lifetime has a significant impact on the pulse shape. After the leading edge of the input pulse saturates the amplifier, the carriers repopulate the active region while the trailing edge of the pulse propagates through the amplifier. When the carrier lifetime is much smaller than the pulse duration, the gain recovers quickly, allowing the leading and trailing edges of the pulse to experience more gain than the center of the pulse. The increased gain experienced by the leading and trailing edges of the pulse results in a broadening that increases the FWHM of the output pulse as compared to the input pulse. As the carrier lifetime increases this effect becomes more pronounced, until the carrier lifetime becomes so long that the leading edge of the input pulse begins to experience more gain than the trailing edge. This yields the asymmetric pulse shape shown for a carrier lifetime of 2.0 ns. As seen in Figure 2 (b), the gain recovery also affects the phase of the output pulse, which is calculated according to Equation (19). The pulse is assumed to have no phase modulation prior to entering the SOA (i.e., $\phi_{in}(t) = 0$). When the carrier lifetime is significantly smaller than the pulse duration, the gain fully recovers, and the phase modulation is symmetric, as seen for a carrier lifetime of 0.1 ns in Figure 2 (b). As the carrier lifetime increases, the duration of the saturation increases, and the gain does not fully recover during the pulse duration. As a result, the magnitude of the phase modulation increases, but the phase modulation becomes asymmetric, as shown for a carrier lifetime of 2.0 ns in Figure 2 (b). Increasing the phase modulation has the effect of increasing the bandwidth of the pulse, as indicated by the pulse spectra of Figure 2 (c). As the carrier lifetime increases and the phase modulation becomes increasingly asymmetric, the spectrum also becomes increasingly asymmetric. The

IPR for each pulse, shown in Figure 2 (d), exhibit sidelobes with peak values on the order of -10 dB. Before examining the IPR in more detail, the effect of the input pulse energy will be explored.

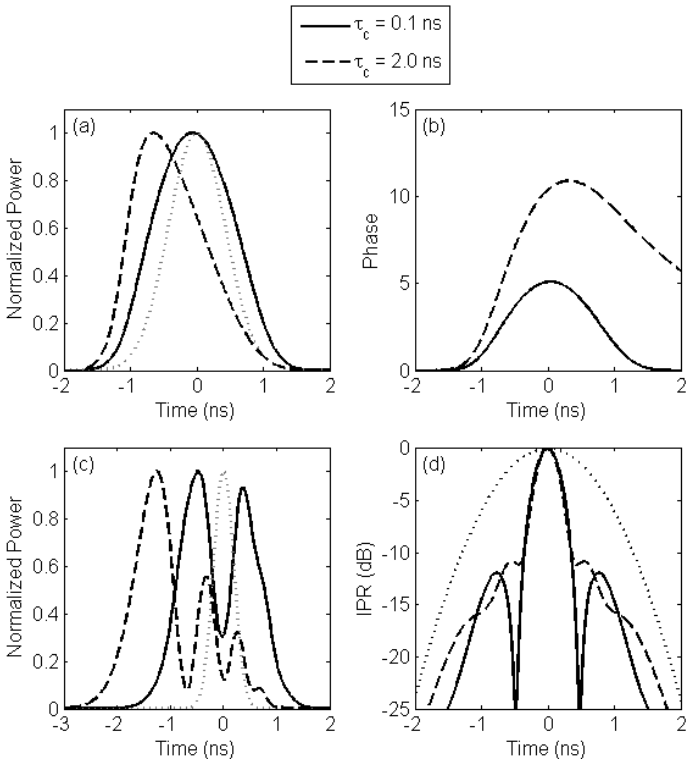

Figure 2. A summary of the impact of the carrier lifetime on the (a) power, (b) phase, (c) pulse spectra, and (d) IPR of the output pulse. This simulation assumes α=6, G_0=30 dB, and a 1 ns FWHM Gaussian pulse at the input to the SOA with an energy one tenth the saturation energy.

Variations in the energy of the input pulse are explored in Figure 3, where a carrier lifetime of 2 ns is assumed. Increasing the energy of the input pulse, shown in Figure 3 (a), results in a sharper leading edge of the output pulse, which increases the FWHM of the output pulse. Increasing the input energy also has the effect of saturating the amplifier earlier in the pulse duration, thus the remainder of the pulse experiences more gain recovery. This results in an increase in the magnitude the phase modulation, as shown in Figure 3 (b). The increase in phase modulation increases the bandwidth of the

pulse, as seen in Figure 3 (c). This results in a narrowing of the IPR, as shown in Figure 3 (d). Note that the peak sidelobes of each IPR remain around -10 dB.

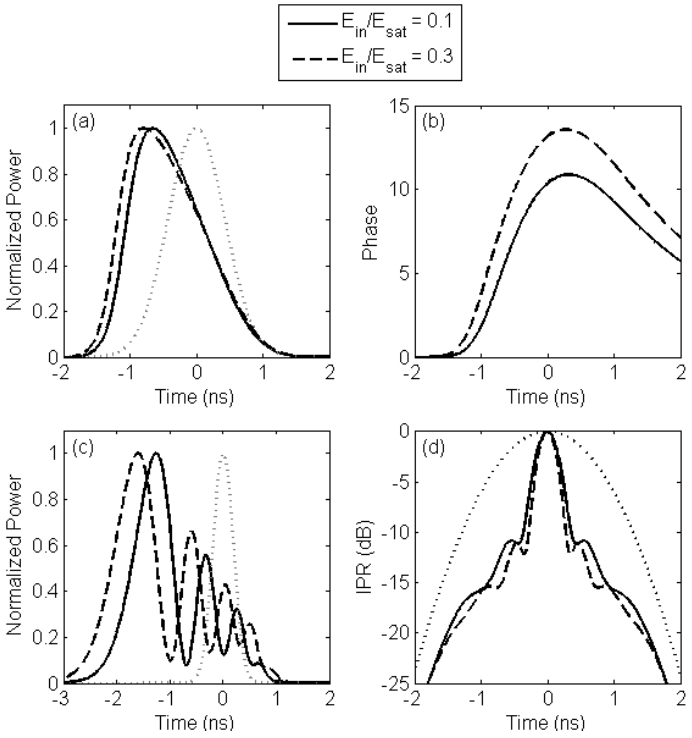

Figure 3. A summary of the impact of the saturation energy on the (a) power, (b) phase, (c) pulse spectra, and (d) IPR of the output pulse. This simulation assumes α=6, G_0=30 dB, τ_c=2.0 ns, and a 1 ns FWHM Gaussian pulse at the input to the SOA.

The effect of the carrier lifetime and input pulse energy on the output pulse is summarized in Figure 4, which shows the FWHM of the output pulse and the saturated gain as a function of carrier lifetime and the ratio of input pulse energy to the saturation energy. As discussed above, for smaller carrier lifetimes, the pulse remains somewhat symmetric, and the FWHM increases as the leading and trailing edges of the pulse experience increased gain with respect to the center of the pulse. However, as the leading edge begins to experience more gain than the trailing edge of the pulse, the FWHM decreases as the output pulse becomes asymmetric. This trend is seen in Figure 4 (a). Increasing the

pulse energy increases the FWHM of the pulse as the leading edge rises more sharply. As shown in Figure 4 (b), increasing the carrier lifetime reduces the amount of gain experienced by the pulse as it takes longer for the gain to recover after saturation. Increasing the input pulse energy also decreases the saturated gain experienced by the pulse as the saturation occurs earlier in the pulse duration.

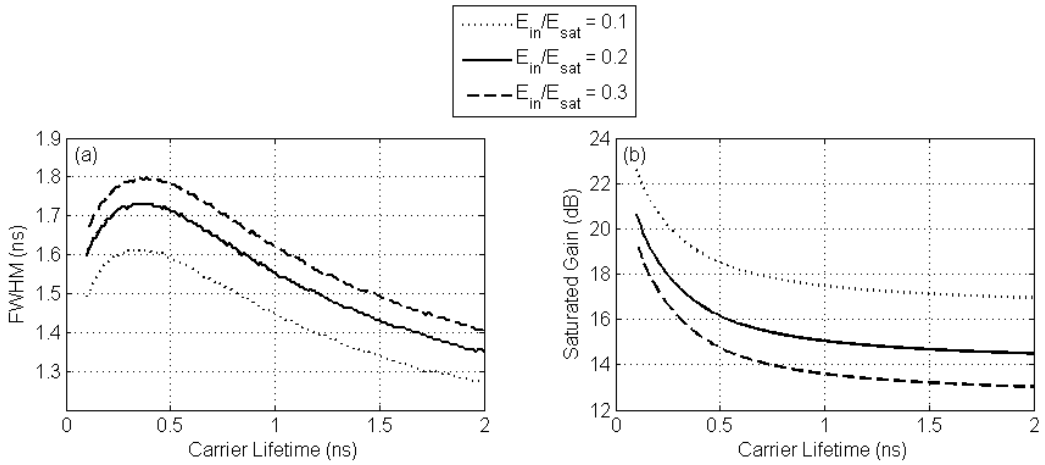

Figure 4. A summary of the (a) FWHM and (b) saturated gain of the output pulse as a function of carrier lifetime and input pulse energy. This simulation assumes α=6 and G_0=30 dB.

The effect of the carrier lifetime and the input pulse energy on the IPR is summarized in Figure 5. Figure 5 (a) shows the range resolution as a function of carrier lifetime, where the range resolution is defined as the 3 dB width of the IPR. As the carrier lifetime increases, the increased gain recovery time increases the magnitude and duration of the phase modulation, which narrows the IPR and improves the range resolution. However, as the carrier lifetime and thus the magnitude of the phase modulation continues to increase, the phase modulation becomes increasingly asymmetric. This asymmetry results in a broadening of the IPR, which degrades the range resolution. The optimum carrier lifetime balances the narrowing of the IPR due to the increased phase modulation with the broadening of the IPR due to

the asymmetric phase modulation. In Figure 5 (a), the optimum carrier lifetime is found to be one half the FWHM of the input pulse, or 0.5 ns.

The IPR is also characterized by the ISLR and PSLR, shown in Figure 5 (b) and (c) respectively. The ISLR decreases as the carrier lifetime increases, and shows very little change as the input pulse energy is varied. This indicates that an increase in carrier lifetime causes the energy within the IPR to spread outside of the 3 dB width of the IPR. The PSLR also shows an overall trend of decreasing with an increasing carrier lifetime, indicating that the peak sidelobe levels slightly increase as the carrier lifetime increases. The variations in the PSLR and ISLR with carrier lifetime are not significant and are seen to be on the order of 1.5 dB. As can be seen, variations in the PSLR and ISLR with input energy are even less significant.

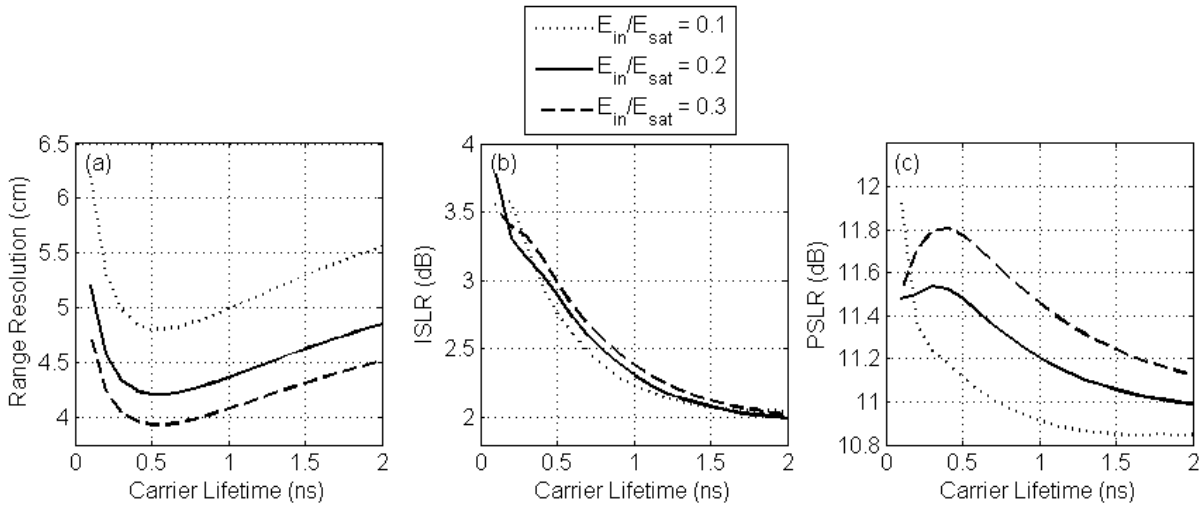

Figure 5. The impact of the carrier lifetime and input pulse energy on the (a) range resolution, which is defined as the 3 dB width of the IPR, (b) ISLR of the IPR, and (c) PSLR of the IPR. This simulation assumes α=6 and G_0=30 dB

Figure 6 further summarizes the effect of the carrier lifetime on the saturated gain. The pulse shapes shown in Figure 4 (a) are normalized to the pulse with the maximum output power (i.e. for τ_c = 0.1 ns) to show the decrease in gain as the carrier lifetime increases. The effects of the decreasing pulse

energies are evident in the spectra, shown in Figure 4 (c), and the IPRs, shown in Figure 4 (d). Results for the optimum carrier lifetime of 0.5 ns are included in this figure. The IPR for τ_c=0.5 ns is a compromise between the phase symmetry for shorter carrier lifetimes, and the increased magnitude of the phase modulation for longer carrier lifetimes, as seen in Figure 4 (b). Note that for a 1 ns FWHM Gaussian input pulse, the pulse emerging from the SOA in this simulation has broadened to a FWHM of 1.6 ns. However, due to the saturation induced phase modulation, the IPR has a 3dB width of 0.32 ns, corresponding to a range resolution of 4.8 cm and a bandwidth of 3.1 GHz.

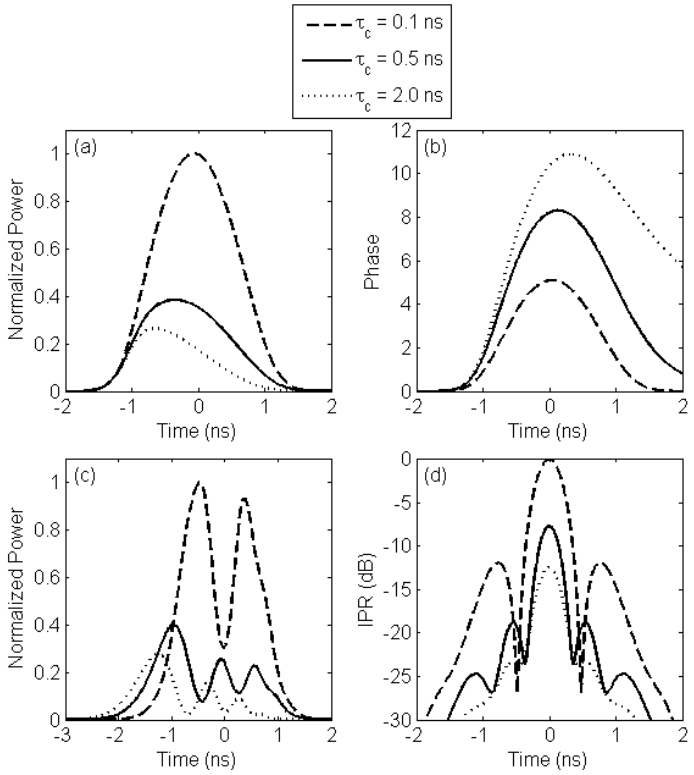

Figure 6. A summary of the impact of the carrier lifetime and saturation energy on the relative gains of a pulse after travelling through the SOA. The (a) power, (b) phase, (c) pulse spectra, and (d) IPR of the output pulse are shown. This simulation assumes α=6, G_0=30 dB, and a 1 ns FWHM Gaussian pulse at the input to the SOA with an energy one tenth the saturation energy. Results for the optimum carrier lifetime of 0.5 ns are presented.

This analysis shows that to optimize range resolution, the optimum carrier lifetime of the SOA is one half the FWHM of the input pulse. Furthermore, a trade-off exists between the increased phase

modulation resulting from increasing the energy of the input pulse with respect to the saturation energy of the SOA, and the decreased gain experienced by the pulse. The ISLR and PSLR of the IPR do not show significant variations with carrier lifetime and input pulse energy.

VII. Effects of the Unsaturated Gain and Chirp Parameter

To explore the effects of the unsaturated gain and the chirp parameter on the output pulse, Equation (22) is once again solved assuming a 1 ns FWHM Gaussian input pulse. All of the simulations in this section will assume an input energy one tenth the saturation energy of the SOA and an optimum carrier lifetime of 0.5 ns. Figure 7 addresses the impact of the unsaturated gain, G_0, for a chirp parameter of 6. As seen in Figure 7 (a), increasing the unsaturated gain of the amplifier increases the gain experienced by the leading edge of the pulse, which results in sharper leading edge and increased asymmetry of the output pulse. Increasing the gain also increases the phase modulation experienced by the pulse, shown in Figure 7 (b). This increases the bandwidth of the pulse, which is evident by the broader spectrum in Figure 7 (c), and narrows the width of the IPR seen in Figure 7 (d).

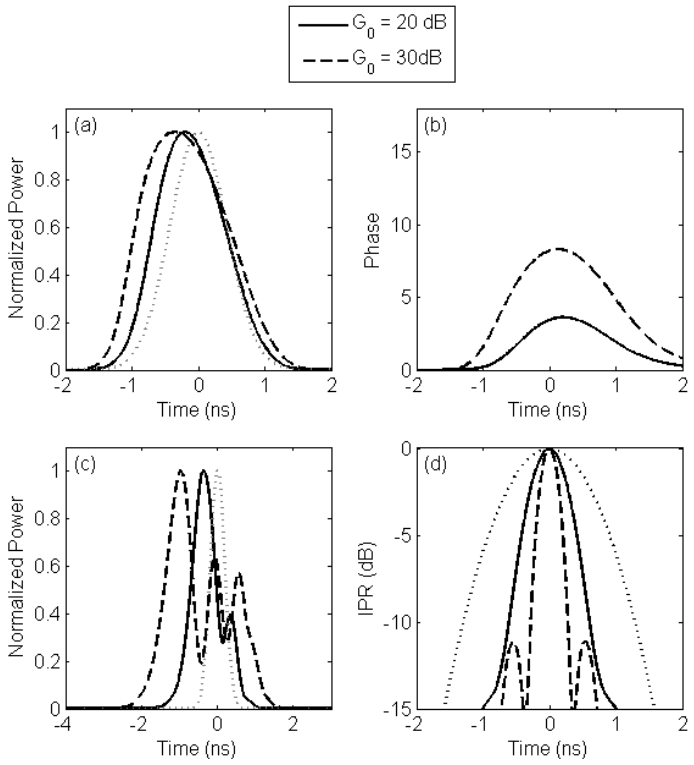

Figure 7. A summary of the impact of the unsaturated gain on the (a) power, (b) phase, (c) pulse spectra, and (d) IPR of the output pulse. This simulation assumes α=6, E_{in}/E_{sat}=0.1, τ_c=2.0 ns, and a 1 ns FWHM Gaussian pulse at the input to the SOA.

The effect of varying the chirp parameter is explored in Figure 8, where an unsaturated gain of 30 dB is assumed. As indicated by Equations (18) and (19), the chirp parameter only affects the phase of the pulse and has no affect on the pulse amplitude. This is reflected in Figure 8 (a), where the pulse profiles are identical for α=2 and α=12. However, the significant effect on the magnitude of the phase modulation is evident in Figure 8 (b). The increased phase modulation broadens the pulse spectrum and narrows the IPR, as seen in Figure 8 (c) and (d) respectively.

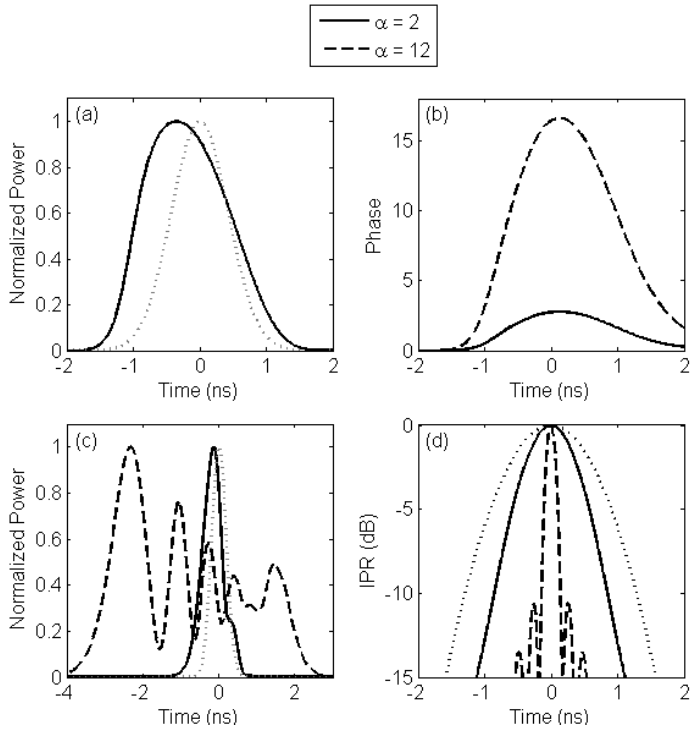

Figure 8. A summary of the impact of the chirp parameter on the (a) power, (b) phase, (c) pulse spectra, and (d) IPR of the output pulse. This simulation assumes G_0=30 dB, E_{in}/E_{sat}=0.1, τ_c=2.0 ns, and a 1 ns FWHM Gaussian pulse at the input to the SOA.

The FWHM and saturated gain as a function of unsaturated gain are shown in Figure 9. Increasing the unsaturated gain also increases the FWHM of the output pulse as the gain experienced by the leading and trailing edges of the pulse increases with respect to the gain experienced by the center of the pulse. The saturated gain as a function of unsaturated gain is shown in Figure 9 (b). Since the chirp parameter affects only the phase and not the magnitude of the pulse, it has no affect on the FWHM or gain of the output pulse.

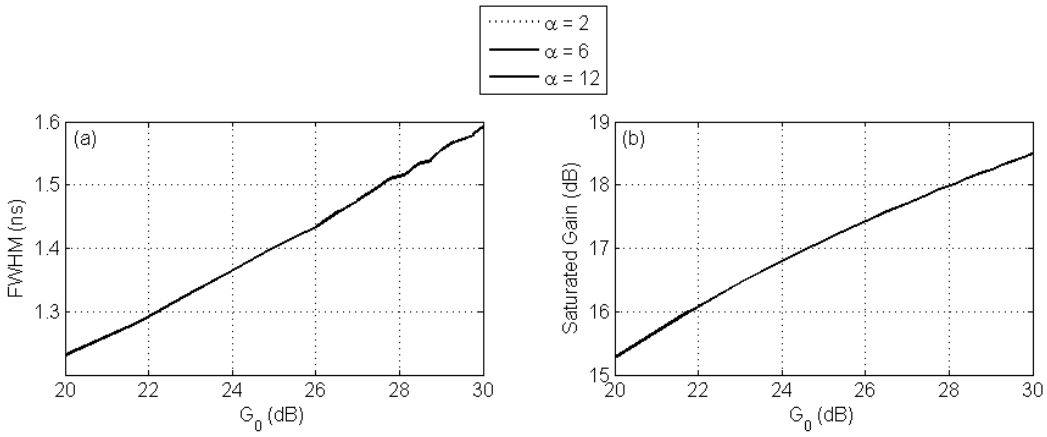

Figure 9. A summary of the (a) FWHM and (b) saturated gain of the output pulse as a function of the unsaturated gain. This simulation assumes τ_c=0.5 ns and E_{in}/E_{sat} = 0.1. The FWHM and saturated gain are not affected by the chirp parameter.

The effect of the unsaturated gain and the chirp parameter on the IPR is summarized in Figure 10. As seen in Figure 10 (a), the range resolution improves with increases in the unsaturated gain or chirp parameter. The ISLR shows less than 1 dB in variation as the unsaturated gain increases, although an increase in chirp parameter from 2 to 12 can cause the ISLR to decrease by roughly 2.5 dB. The PSLR is shown only for cases where there are discernable peaks. For instance, in Figure 8 (d) the IPR has no discernable peaks when α = 2. As can be seen, the PSLR shows no more than 2 dB of variation as the unsaturated gain is increased.

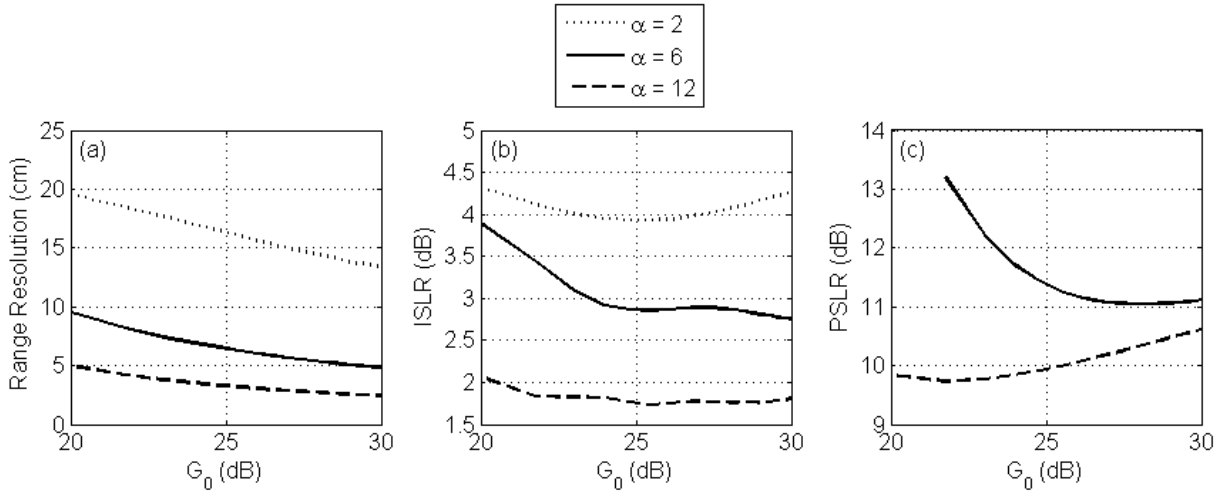

Figure 10. The impact of the saturated gain and chirp parameter on the (a) range resolution, which is defined as the 3 dB width of the IPR, (b) ISLR of the IPR, and (c) PSLR of the IPR. This simulation assumes τ_c=0.5 ns and E_{in}/E_{sat}=0.1.

This analysis shows that in order to optimize the range resolution and saturated gain experienced by the pulse, it is advantageous to choose a SOA with maximum unsaturated gain and chirp parameter values. Although the range resolution increases significantly as the chirp parameter is increased, this does have the negative impact of decreasing the ISLR and PSLR of the IPR.

VIII. Discussion

The above analysis has investigated the characteristics of a SOA and their impact on the IPR of a laser radar system. Based on the analysis presented above, we will assume the SOA parameters summarized in Table 2 for a 1 ns FWHM Gaussian input pulse. The carrier lifetime of 0.5 ns was found to optimize the range resolution of the system. An unsaturated gain of 30 dB is assumed, and an input energy such that E_{in}/E_{sat} = 0.1 would allow for significant phase modulation while also providing a saturated gain of approximately 18.5 dB, as shown in Figures 4 (b) and 9 (b). If the source cannot emit pulses with sufficient energy to saturate the amplifier, it is assumed that additional optical amplifiers could be employed prior to the SOA shown in Figure 1 (b) to achieve the necessary input energy, provided that the additional amplifiers are not saturated and do not result in any appreciable phase modulation prior to the saturated SOA. A chirp parameter of 6 is assumed to be reasonable as it is between the minimum value of 2 and the maximum value of 12 cited in the literature[4].

Table 2. SOA Parameters Simulated for Experimental Demonstration

SOA Parameters			Output Pulse Parameters		
Variable	**Designation**	**Value**	**Variable**	**Designation**	**Value**
Input Pulse FWHM	τ_p	1 ns	Output Pulse FWHM	$\tau_{p,o}$	1.6 ns
Carrier Lifetime	τ_c	0.5 ns	Saturated Gain	G	18.5 dB
Unsaturated Gain	G_0	30 dB	Range Resolution	ΔR	4.8 cm
Ratio of Input Energy to Saturation Energy	E_{in}/E_{sat}	0.1	Integrated Sidelobe Level Ratio	ISLR	2.55 dB
Chirp Parameter	α	6	Peak-to-Sidelobe Level Ratio	PSLR	11.1 dB

A pulsed source will experience some variation in pulse duration and energy. The effect of a ±10% variance in pulse duration or energy on the IPR of the transmitted pulse is summarized in Figure 11. In each case, it is assumed that the output of the SOA has been monitored and is used as the matched filter, therefore the matched filter accounts for the variations in pulse duration and energy. Assuming the SOA parameters outlined in Table 2, a ±10% change in pulse duration for a 1 ns FWHM Gaussian pulse affects the range resolution by ±10%. For a pulse duration of 1 ns, a ±10% change in input energy affects the range resolution by ±2%. Note that the SOA is much more sensitive to changes in pulse duration than variations in pulse energy. However, even the variations in pulse duration do not have a significant impact on the IPR. A transform limited pulse with variations of ±10% in pulse duration would also experience variations of ±10% in range resolution as determined by Equation (1). This suggests that for a reasonably stable source a monitor may not be necessary, as the IPR does not change significantly with variations of the input pulse duration or energy.

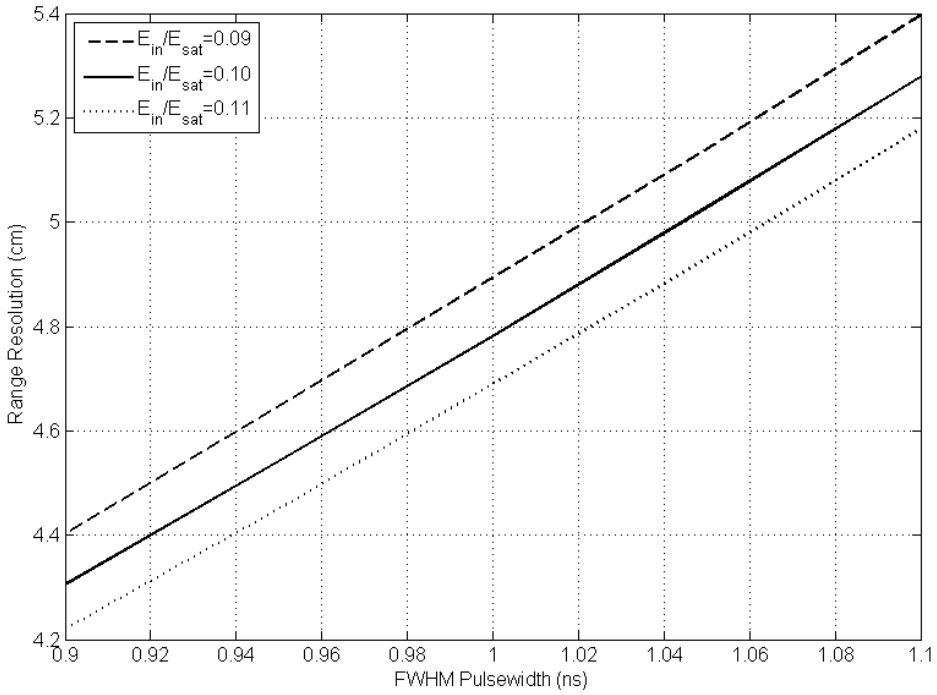

Figure 11. Summary of the impact of 10% variations in the input pulse duration and energy for the SOA parameters outlined in Table 2. In each case, the matched filter is adjusted to account for these variations.

If a single matched filter is constructed using the SOA parameters outlined in Table 2, the matched filter output for pulses with varying pulse durations and input energies are shown in Figure 12. In this case, the matched filter will not account for variations in the transmitted pulse. In each plot, the solid line represents the IPR where the matched filter is perfectly matched to the received signal for τ_p = 1 ns and E_{in}/E_{sat}=0.1. Variations in the pulse duration result in an asymmetric matched filter output, as seen in Figure 12 (a), but little change in the 3 dB width of the matched filter output as compared to the IPR. As indicated in Figure 12 (c), a change in pulse duration of ±10% yields a 0.4 dB variation in ISLR and a 0.48 cm variation in range resolution. It can be deducted from Figure 12 (a) that variations in the sidelobe levels are much less than 1 dB, and therefore any change in the PSLR is considered insignificant. However, it is evident that the peak of the IPR shifts slightly in time as the duration of the output pulse varies, which will yield an error in the range measurement. This is summarized in Figure 13, which

shows that range errors on the order of ±0.5 cm could be expected for ±10% variations in the pulse duration.

The impact due to ±10% variations in the pulse energy, as shown in Figure 12 (b), is much less noticeable. According to Figure 12 (d), this yields a 0.01 dB variation in ISLR and a 0.10 cm variation in range resolution. Once again, changes in the PSLR are judged to be insignificant by inspection of Figure 12 (b). Therefore, mismatches between the return signal and the matched filter due to variations in the pulse energy or duration at the input to the SOA do not produce significant variations in the matched filter output. This confirms that for a stable pulsed source with duration and energy variations on the order of ±10%, there is little error introduced if the matched filter is constructed for the ideal case rather than from monitoring the variations in each transmitted pulse.

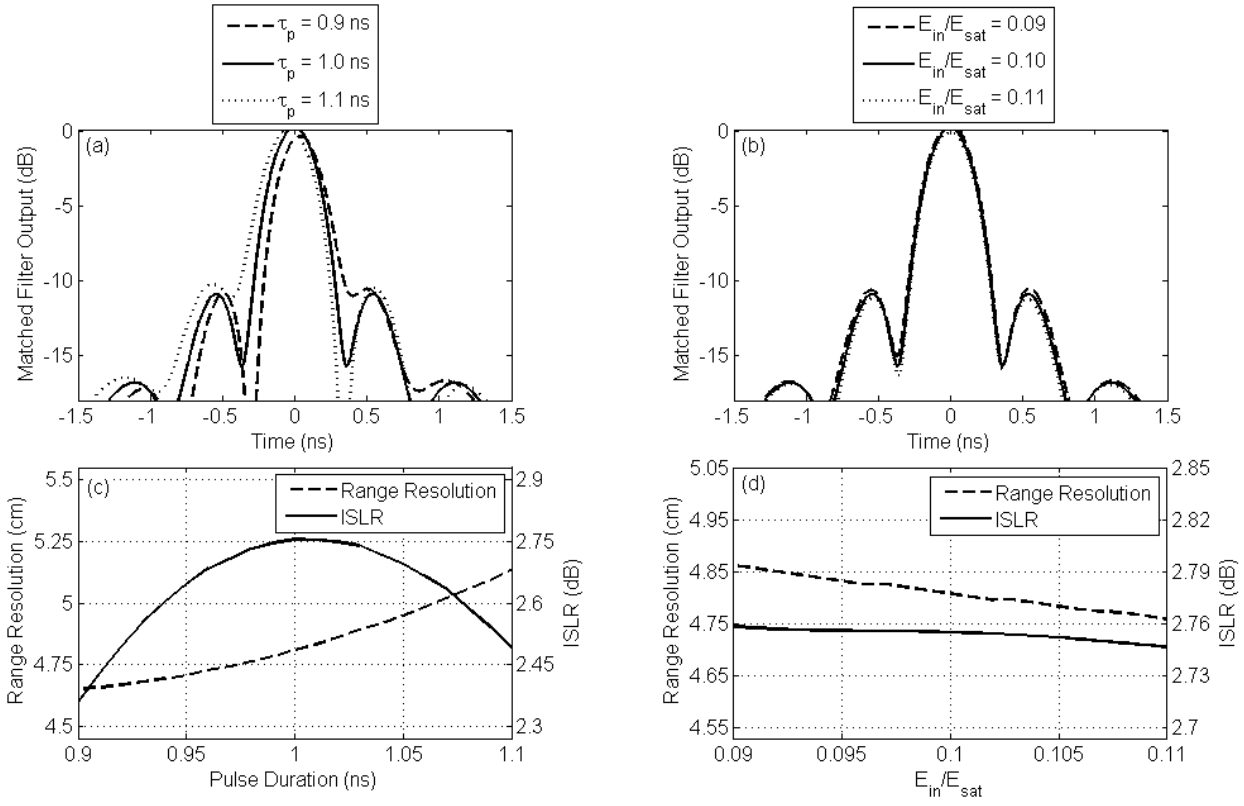

Figure 12. Effect of variations in input pulse duration and input energy on the matched filter output for the SOA parameters outlined in Table 2. In each case, the matched filter is fixed and assumes an input pulse duration of τ_p=1 ns and input pulse energy of E_{in}/E_{sat} = 0.1.

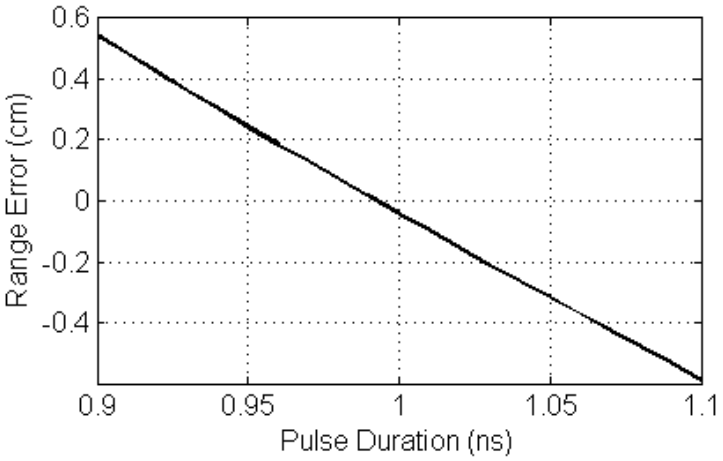

Figure 13. Range error as a function of variations in input pulse duration for the SOA parameters outlined in Table 2.

As discussed above, the primary motivation for this work is to investigate methods that enable the transmission of high bandwidth pulses that are also shorter in duration than those typically used, thereby minimizing the detrimental effects due to target motion. Figure 8 offers a comparison of the IPR obtained using the parameters outlined in Table 2 to those obtained using the longer duration (here, 20 μs) LFM pulses that are typically employed. The IPR for a transform limited Gaussian pulse is also included for reference. The characteristics of each pulse are summarized in Table 3. In each case, the 3 dB widths of the main lobe are identical. The ISLR for the amplifier modulated pulse is degraded by about 2.2 dB as compared to the transform limited pulse, and by about 1.4 dB as compared to the LFM pulse. The largest sidelobe is about 2 dB higher for the SOA-modulated pulse than the traditional LFM pulse.

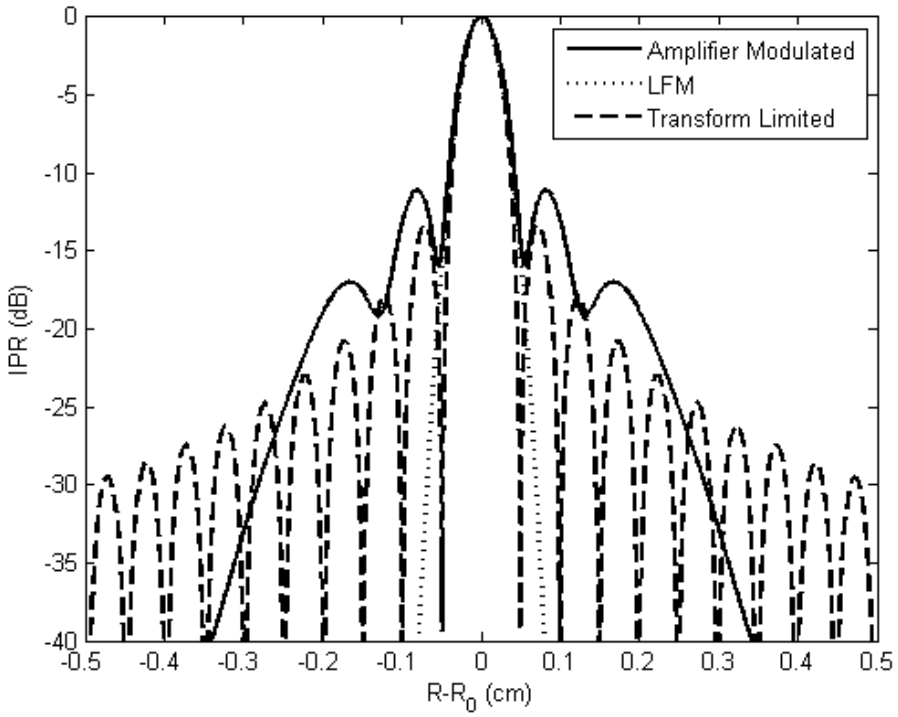

Figure 14. IPRs for an amplifier modulated pulse, a 20 μs LFM pulse, and a transform limited Gaussian pulse, all with a range resolution of 4.8 cm. The highest sidelobe level for the amplifier modulated IPR is 2 dB higher than that of the traditional LFM pulse.

Table 3. Comparison of amplifier modulated, LFM, and transform limited Gaussian pulses

	Amplifier Modulated	LFM	Transform Limited
FWHM	1.6 ns	20 μs	0.22 ns
ΔR	4.8 cm	4.8 cm	4.8 cm
ISLR	2.58 dB	4.02 dB	4.80 dB
PSLR	11.1 dB	13.3 dB	n/a

The above analysis assumes a 1 ns FWHM Gaussian input pulse, with the saturation-induced phase modulation improving the range resolution beyond the 15 cm requirement presented in Table 1. The use of the SOA as both an amplifier and a phase modulator can also serve to relax the source

requirements by allowing the use of a longer input pulse duration that is modulated to provide the necessary 15 cm range resolution. To explore this option, Equations (18) through (20) were solved for various pulses with the same energy but different pulse durations. The range resolution of the resulting transmitted pulse as a function of the input pulse duration is shown in Figure 15 (a) for G_0=30 dB and E_{in}/E_{sat} = 0.1. The carrier lifetime was optimized to be one half of each pulse duration, representing the best case scenario for range resolution. As expected, the required pulse duration is heavily dependent on the chirp parameter of the SOA. For a chirp parameter of α=6, an input pulse with a FWHM of 3.1 ns would meet the 15 cm range resolution requirement, while a SOA with α=12 would allow an input pulse duration of 6.3 ns. As shown in Figure 15 (b), the ISLR remains relatively stable as the input pulse duration increases. The PSLR shows some improvement as the pulse duration increases, as seen in Figure 15 (c), but the significant improvements only occur once the pulse duration has increased to the point that the subsequent range resolution is greater than 15 cm. Note that there are no discernable peaks in the IPR for α=2.

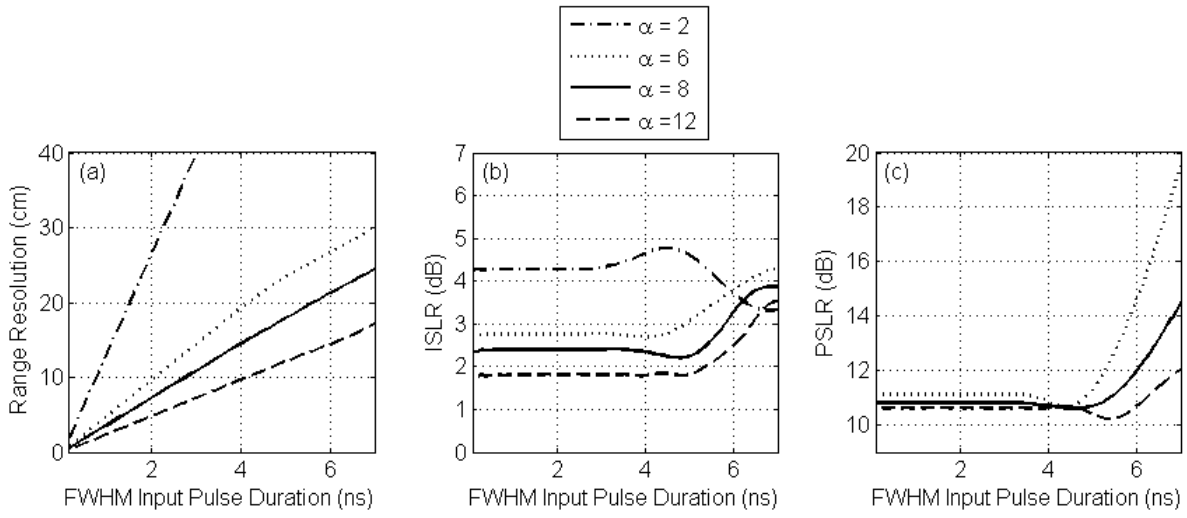

Figure 15. The (a) range resolution, (b) ISLR, and (c) PSLR of the saturation induced phase modulated pulse as a function of the input pulse duration for varying chirp parameters, assuming G_0 = 30 dB and E_{in}/E_{sat} = 0.1. The optimum carrier lifetime for each pulse duration was used in this simulation.

This analysis has shown that the phase modulation induced by a saturated SOA can be exploited as additional bandwidth to improve the range resolution of a laser radar system. The following section will present proof of concept laboratory results for the transmission of pulses with a phase modulation characteristic of what would be expected from a saturated SOA.

IX. Experimental Results

The effect of the SOA on the transmitted pulse was simulated in the lab using the setup detailed in Figure 16. Limitations in the speed of the available digitizers limited the pulse bandwidth that could be accurately sampled, so instead of directly saturating a SOA this process was simulated by replacing the components within the dashed box in Figure 1 (b) with those seen in the dashed box in Figure 16. This allowed the output pulse to be broadened in time, reducing the bandwidth of the received pulse and thus the speed at which the received signal must be sampled. The setup is described in detail below.

The source is a CW 1.55 μm NP Photonics fiber laser. The first beam splitter (BS) picks off a portion of the beam to serve as a local oscillator (LO). A Brimrose 500 MHz acousto-optic modulator (AOM) serves as an amplitude modulator by sending one channel of the Tektronix arbitrary waveform generator (AWG) through an amplifier (not shown) to drive the AOM at its resonant frequency for a short period of time, thereby pulsing the transmitted signal. The amplitude of the resonant frequency was adjusted to yield the pulse profile for the SOA described in Table 2. The AOM also serves to offset the transmitted signal from the LO slightly in frequency. A second channel of the AWG passes through an amplifier to drive an EOspace low V_π Lithium Niobate phase modulator (PM) that is used to simulate

the phase modulation of a saturated SOA. The amplitude of the drive signal was adjusted to yield the desired phase profile. Before transmission, a portion of the signal is picked off to serve as a monitor. Upon receipt, the return signal is intercepted by a transmit receive switch (Tx/Rx). Two free space I/Q demodulators are used to detect the monitor and received signal, each containing a quarter waveplate ($\lambda/4$) and a half waveplate ($\lambda/2$) to yield a circularly polarized LO and a signal/monitor polarized at 45 degrees, as discussed in Section III. The I/Q demodulator combines the LO and signal/monitor with a beamsplitter and then separates the signal into I and Q components using a polarized beamsplitter (PBS). The I and Q components of the monitor are measured using fiber-coupled 12-GHz 1544-B New Focus detectors (D_1 and D_2), and the I and Q components of the signal are measured using identical detectors (D_3 and D_4). A 4-channel Acqiris DC282 Digitizer was used to collect the data at a rate of 2 gigasamples/second. The AOM did not have a fast enough response time to allow for the transmission of the 1.6 ns FWHM pulse seen in Figure 6 (a). As such, the transmitted pulse duration and phase modulation was slowed down by a factor of 25 to accommodate the response time of the AOM.

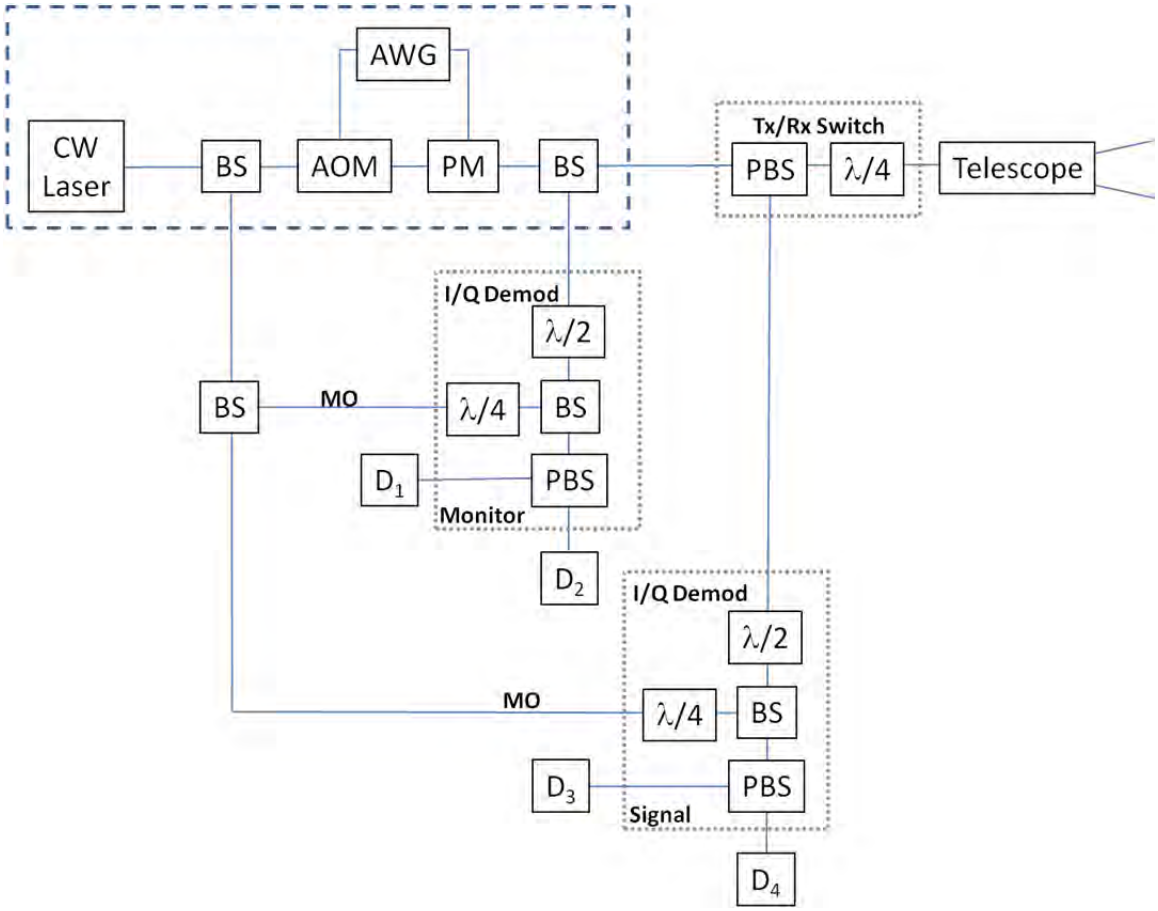

Figure 16. Laboratory setup used to simulate saturation induced modulation in Gaussian pulses.

This setup was first used to obtain data from a corner cube attached to a Hardy vibration calibration stand. An example of the power, phase, and IPR of a received pulse is shown in Figure 17. The theoretical data is represented by the dotted line. As can be seen, the transmitted pulse closely approximates the characteristics of the simulated pulse. Vibration data was collected with the calibration stand set to 1075 Hz, 3001 Hz, and 848 Hz. The data was processed as outlined in Section IV, and the Fourier transform of the phase history is presented in Figure 18. The measured vibration frequencies match the known values as reported by the Hardy vibration calibration stand.

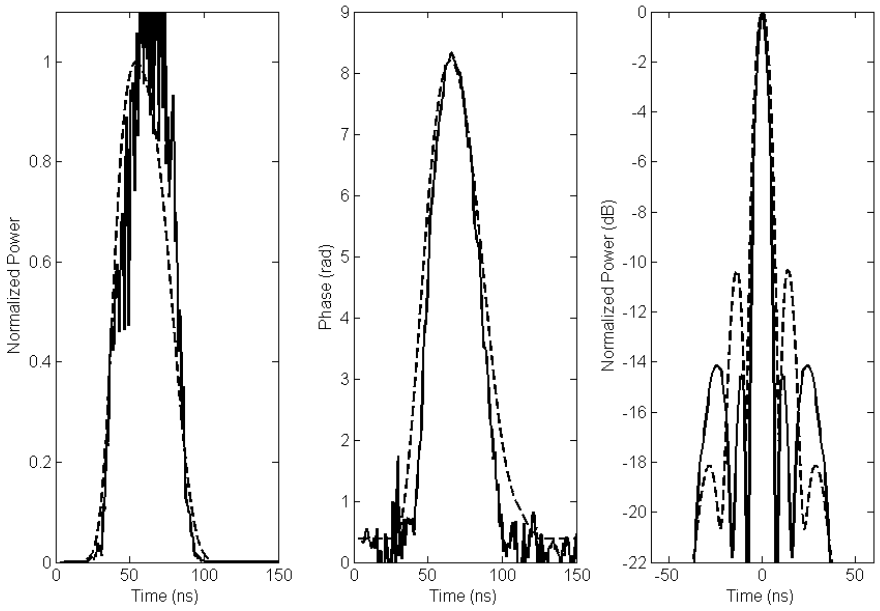

Figure 17. Experimental (solid line) and theoretical (dashed line) results for the (a) pulse profile, (b) phase modulation, and (c) IPR of Gaussian pulses with a phase modulation characteristic of a saturated SOA.

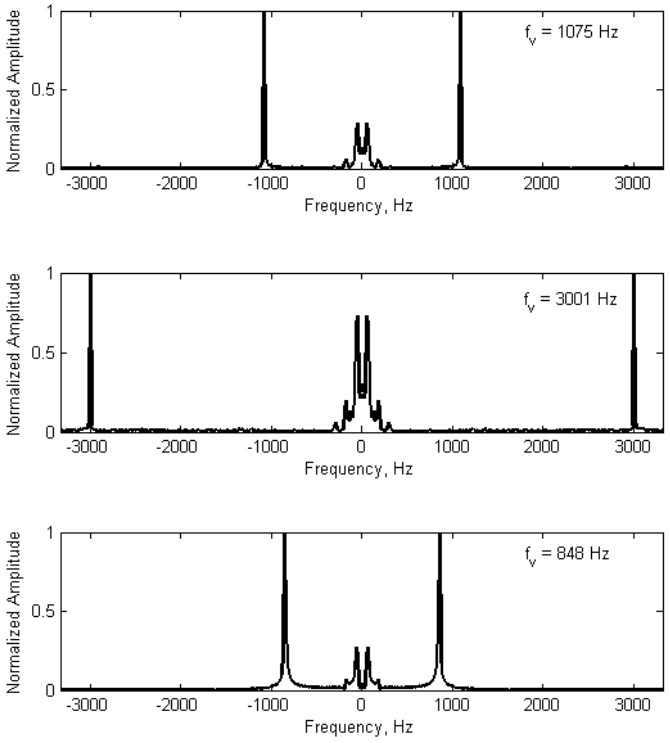

Figure 18. Processed vibrometry data for a corner cube vibrating at 1075 Hz (top), 3001 Hz (middle) and 848 Hz (bottom). The data was obtained using pulses with a phase modulation characteristic of a saturated SOA.

This setup was also used to obtain data from a translating target, which was a corner cube attached to a pendulum. For this data set, a 3 inch telescope was placed behind the transmit/receive switch. The data was processed as outlined in Section IV, and the results are presented in Figure 19. Figure 19 (a) shows the received signal power as a function of fast and slow time. Figure 19 (b) is the result after the fast-time matched filter is applied, showing compression in the fast-time domain. Figure 19 (c) is the result after the full 2-D matched filter has been applied, which yields the location of the corner cube in fast-time (range) and slow-time (cross-range). A cross-section of the matched filter output in fast-time and slow-time are shown in Figure 19 (d) and (e), respectively. Here, the dotted lines represent the theoretical results. As can be seen, the experimental results closely match the theoretical results, although the experimental results experience higher noise levels.

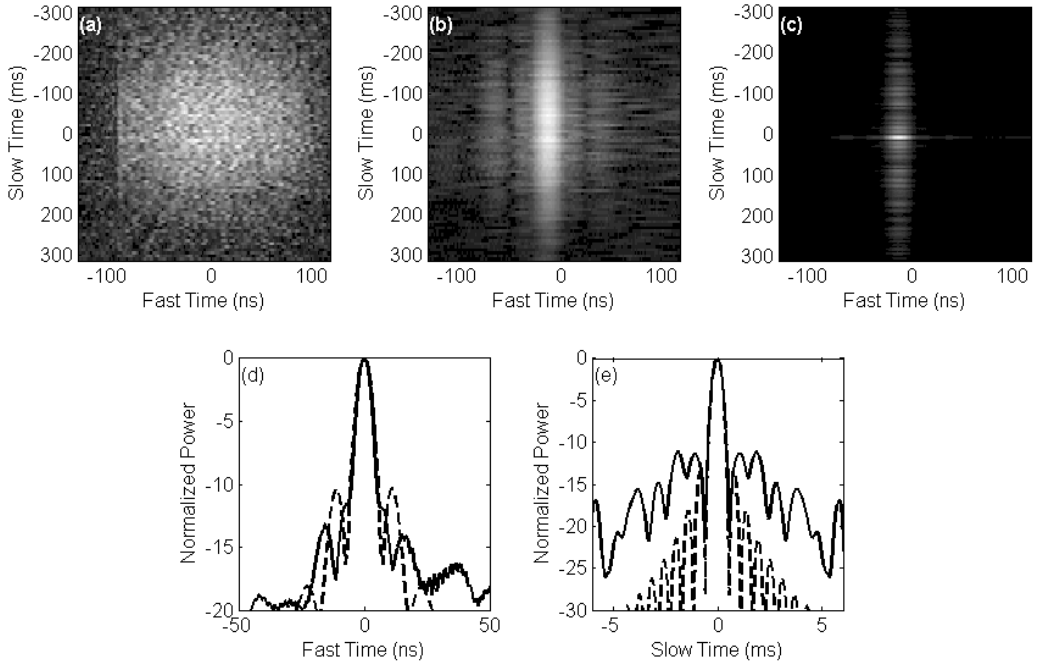

Figure 19. Processed SAL data for a corner cube attached to a pendulum. The (a) received signal power, (b) output of the fast-time matched filter, and (c) subsequent output of the slow-time matched filter are presented. A cross-section of the 2-D matched filter output is shown in (d) fast-time and (e) slow-time for both experimental (solid line) and theoretical (dotted line) data. The data was obtained using pulses with a phase modulation characteristic of a saturated SOA.

This proof of concept experiment shows that pulses with the phase and amplitude modulation expected from a saturated SOA can be collected from vibrating and translating targets, and compressed via matched filtering techniques to yield the location of the target in range.

X. Conclusion

By exploiting the saturation induced phase modulation of a SOA as bandwidth, the range resolution of a laser radar system can be improved, or the pulse duration requirements of the transmitter can be relaxed. The phase modulation depends on the carrier lifetime, saturation energy, unsaturated gain, and chirp parameter of the SOA. An optimum carrier lifetime exists for a given input pulse duration, striking a balance between the increased bandwidth due to increasing the magnitude of the phase modulation, and the broadening of the IPR due to the asymmetry of the phase modulation. For a nominal matched filter, variations in the pulse duration or pulse energy on the order of ±10% do not significantly degrade the matched filter response. Exploiting the phase modulation induced by the SOA allows the SOA to serve two purposes, amplifying and modulating the transmit pulse. As compared to traditional techniques using LFM pulses on the order of tens of microseconds in duration, this allows for the transmission of shorter pulses that are less sensitive to target motion, and eliminates the need for hardware associated with LFM. However, the IPR experiences higher sidelobe levels and a decreased ISLR as compared to the IPR for traditional LFM. The phase modulation, amplitude modulation, and resulting fast-time IPR for a notional SOA were presented and simulated in a laboratory demonstration using a vibrating target and a translating target.

This effort was supported in part by the United States Air Force Research Laboratory and the Ladar and Optical Communications Institute (LOCI) at the University of Dayton. The authors wish to

thank Lawrence Barnes, of the Air Force Research Laboratory, and John Schmoll and Timothy Meade, of OptiMetrics, Incorporated, for their valuable contributions to this research.

The views expressed in this article are those of the authors and do not reflect on the official policy of the Air Force, Department of Defense, or the United States government.

VI. References

1. J. Ricklin, B. Schumm, and P. Tomlinson, "Synthetic aperture ladar for tactical imaging (SALTI) flight test results and path forward," presented at the Coherent Laser Radar Conference, Snowmass, CO (9–13 July 2007).

2. Kopeika, Norman S. A System Engineering Approach to Imaging. SPIE, 1998.

3. Richards, Mark A. Fundamentals of Radar Signal Processing, McGraw Hill, 2005.

4. Agrawal, Govind P. "Self-phase modulation and spectral broadening of optical pulses in semiconductor optical amplifiers," IEEE J. of Quant. Elec., 25(11), 2297-2306, Nov 1989.

5. Storkfelt, N., B. Mikkelsen, D.S. Olesen, M. Yamaguchi, and K. E. Stubkjaer, "Measurement of Carrier Lifetime and Linewidth Enhancement Factor for 1.5-mm Ridge-Waveguide Laser Amplifier," IEEE Phot Tech Lett, 3(7), 1991, 632-634.